ELSEVIER

Journal of Chromatography A, 686 (1994) 179–192

JOURNAL OF CHROMATOGRAPHY A

Sorption kinetics and breakthrough curves for pepsin and chymosin using pepstatin A affinity membranes

Shing-Yi Suen[a,1], Mark R. Etzel[b,*]

[a]*Department of Chemical Engineering, 1415 Johnson Drive, University of Wisconsin, Madison, WI 53706-1619, USA*
[b]*Department of Food Science, 1605 Linden Drive, University of Wisconsin, Madison, WI 53706-1519, USA*

First received 24 May 1994; revised manuscript received 26 July 1994

Abstract

Isotherms and kinetic parameters for pepsin and chymosin sorption to immobilized pepstatin A were measured in batch experiments. The measured single-solute parameters were used in an affinity-membrane model which included competitive sorption kinetics, axial diffusion and dead volume mixing. The predictions made using the affinity-membrane model matched the experimental breakthrough curves, whereas predictions made using local-equilibrium theory were a distinct mismatch. The performance of affinity-membrane separations was dominated by slow sorption kinetics.

1. Introduction

Among the bioseparation techniques available today, affinity separations are popular due to their simplicity and high degree of specificity. Conventionally, affinity separations are carried out in columns packed with porous beads to which the ligand is immobilized. The desired biomolecule adsorbs to the ligand via a specific binding recognition, and is separated from the solution. In general, the adsorption rate in columns is limited by either slow intraparticle diffusion for large beads, or low axial velocities and high pressure drops for small beads [1,2]. These limitations result in long cycle times or low throughputs, both of which are economically unattractive. To overcome these limitations, affinity membranes, which utilize convection through the fine pores of the membrane, were recently introduced [2,3]. The advantages of adsorptive-membrane separations have been shown in previous experimental studies [3–7].

In our previous work [8,9], single-solute and multi-solute mathematical models were established to describe the performance of affinity membranes. The effects of axial diffusion, flow velocity and sorption kinetics on separation performance were discussed. It was found that axial diffusion, which is insignificant in affinity column separations, may dominate over convection at low flow-rates or for thin membranes. On the other hand, at high flow velocities, some solutes may pass directly through the membrane without binding due to slow sorption kinetics. Sorption kinetics were shown to dominate affinity-membrane performance. Slow sorption

* Corresponding author.
[1] Present address: Department of Chemical Engineering, National Chung Hsing University, Taichung, Taiwan.

0021-9673/94/$07.00
SSDI 0021-9673(94)00701-2

kinetics may explain the elution peak broadness for increased flow-rate reported by Briefs and Kula [3], and the reduction in ligand capture efficiency at high flow-rates presented by Nachman et al. [10]. Considering the extremes defined by the effects of axial diffusion and sorption kinetics, there should exist a suitable flow-rate range for optimal performance in affinity-membrane separations. Such an optimal flow-rate was found experimentally by Josić et al. [5], and supports these model predictions.

Our theoretical model was used to determine that a small variation in either thickness or porosity may cause a significant degradation in separation performance. As a result, the use of stacked membranes was proposed to avoid these problems. Josić et al. [5] and Liu and Fried [11] studied the influence of membrane thickness experimentally and verified this proposal. Kim et al. [12] indicated that the dispersion in their experimental breakthrough curves may be due to the effect of residence time distribution resulting from pore size distributions.

In 1994, Liu and Fried [11] adapted our theoretical model to analyze their experimental breakthrough curves using Cibacron Blue 3GA–cellulose affinity-membrane separations. However, they did not directly compare their experimental results with predictions from our theoretical model. Also in 1994, Serafica et al. [13] adapted our model to analyze their experimental breakthrough curves using metal chelate affinity membranes with a hollow-fiber geometry. The experimental and modeling results were in good agreement at low effluent concentrations, but showed a discrepancy at high concentrations. It should be noted that the above studies primarily concerned single-solute performance.

The binary-solute affinity-membrane model in our previous work [9] described competition and interference effects between solutes due to differences in either sorption kinetics or isotherms. The purpose of this study was to validate the affinity-membrane model using experimental results. The system of pepsin and chymosin was chosen for study. The sorption kinetic and equilibrium parameters of pepsin and chymosin to affinity membranes containing immobilized pepstatin A were measured in batch adsorption experiments. These parameters were used in our affinity-membrane model to provide an independent and quantitative validation of the model by comparison to experimental breakthrough curves.

2. Affinity-membrane model

The equation of continuity for solute i was [8,9]:

$$\frac{\partial C_i}{\partial \tau} + \frac{\partial C_i}{\partial \zeta} + m_i \cdot \frac{\partial C_{s,i}}{\partial \tau} - \frac{1}{Pe_i} \cdot \frac{\partial^2 C_i}{\partial \zeta^2} = 0 \qquad (1)$$

where axial diffusion was characterized by the axial Peclet number, Pe_i. Eq. 1 quantified changes in solute concentration with time due to solute convection, sorption and diffusion. For adsorption in the loading stage, the multi-solute Langmuir sorption model was used to describe the binding kinetics between solute i and the ligand:

$$m_i \cdot \frac{\partial C_{s,i}}{\partial \tau} = n_i \left[C_i \left(1 - \sum_j C_{s,j} \right) - \frac{C_{s,i}}{r_i - 1} \right] \qquad 0 < \tau \leq \tau_w \qquad (2)$$

where τ_w is the time at which washing starts.

Two models were developed for the washing stage in affinity-membrane separations. First, association and dissociation were assumed to occur during washing. In this work, loading buffer was used as washing buffer. This presented the same environment for protein sorption during the washing stage as existed during the loading process. Therefore, the adsorption equation for loading was used for washing,

$$m_i \cdot \frac{\partial C_{s,i}}{\partial \tau} = n_i \left[C_i \left(1 - \sum_j C_{s,j} \right) - \frac{C_{s,i}}{r_i - 1} \right] \qquad \tau > \tau_w \qquad (3)$$

In the second model, no adsorption and desorption was assumed in the washing stage,

$$m_i \cdot \frac{\partial C_{s,i}}{\partial \tau} = 0 \quad \tau > \tau_w \qquad (4)$$

The initial conditions were set such that there was no solute in the membrane:

$$C_i = 0 \text{ at } \zeta \geq 0,\ \tau = 0 \tag{5}$$

$$C_{s,i} = 0 \text{ at } \zeta \geq 0,\ \tau = 0 \tag{6}$$

In order to include axial diffusion at the front surface of the membrane, and instantaneous mixing at the exit of the membrane, Danckwerts' boundary conditions [14] for frontal chromatography were used:

$$C_i - \frac{1}{Pe_i} \cdot \frac{\partial C_i}{\partial \zeta} = 1 \text{ at } \zeta = 0,\ 0 < \tau \leq \tau_w$$

$$= 0 \text{ at } \zeta = 0,\ \tau > \tau_w \tag{7}$$

$$\frac{\partial C_i}{\partial \zeta} = 0 \text{ at } \zeta = 1,\ \tau > 0. \tag{8}$$

During the washing step, the second form of Eq. 7 was used wherein no protein was fed into the system. The PDASAC software package [15] was used to solve Eqs. 1–8.

3. Experimental

3.1. Materials

Immobilon AV (IAV) affinity membranes were purchased from Millipore (Bedford, MA, USA). The average membrane pore size was 0.65 μm [16]. The IAV membranes were cut into discs of 47 mm diameter. A membrane holder (Product No. 11101) was obtained from Amicon (Beverly, MA, USA). Porcine pepsin (P6887), pepstatin A (P4265), 1,6-hexanediamine (H2381) and dichlorotriazinylaminofluorescein (DTAF, D0531) were purchased from Sigma (St. Louis, MO, USA). Recombinant chymosin (CHY-MAX) was a gift from Pfizer (Milwaukee, WI, USA). The buffer for loading and washing was 0.01 *M* imidazole with 1 *M* NaCl, pH 6 [17–19]. The elution buffer was 0.01 *M* sodium phosphate, pH 12. Chymosin was dialyzed with 12 000 MWCO cellulose tubing (Sigma) against loading buffer to remove unwanted salts. Dialyzed chymosin was used directly without further concentration. All buffers and liquid solutions contained the preservative sodium azide 0.005% and were vacuum-filtered with 0.2-μm filters (Supor 200; Gelman Sciences, Ann Arbor, MI, USA). Protein solutions were made with the loading buffer and filtered with 0.45-μm filters (F9888, Sigma). All solutions were vacuum degassed prior to use.

3.2. Properties of pepsin and chymosin solutions

The system studied in this work was soluble pepsin (EC 3.4.4.1) and chymosin (EC 3.4.4.15) bound to immobilized pepstatin A. Reasons for using this system were: (1) the biophysical properties of chymosin and pepsin are well-known [18,20–22] (see Table 1), (2) the equilibrium and kinetic properties of this system have been studied using gel beads [17–19], (3) binding to the ligand is monovalent [17–19] and (4) competitive and interactive sorption was exhibited for this system in our previous theoretical study of binary-solute affinity-membrane separations [9].

Pure and mixed solutions of chymosin and pepsin were held at pH 6 in order to prevent proteolysis and yet maintain affinity binding. Both pepsin and chymosin are acid proteases which are active only in acidic environment

Table 1
Properties of pepsin and chymosin solutions

	Pepsin	Chymosin	Ref.
M_r	34 500	33 500	18
$E^{280\text{ nm}}_{1\text{ mg/ml}}$	1.44 (pH 6)	1.16 (pH 6)	18
pI	< 1.0	4.5	20
$D_{20,w}$ (cm^2/s)	$8.71 \cdot 10^{-7}$ (pH 6)	$8.5 \cdot 10^{-7}$ (pH 5.8)	21, 22

[20,21]. Mixtures of pepsin and chymosin are stable between pH 5 and 6 [20]. Denaturation occurs rapidly at higher pH.

The stability of pure and mixed solutions of pepsin and chymosin at pH 6 was confirmed by HPLC analysis (data not shown). The HPLC system consisted of a pump (Model 2350; ISCO, Lincoln, NE, USA), a detector (Model V^4, ISCO) and a size-exclusion column (300 mm × 7.8 mm Bio-Sil SEC-125 with 80 mm × 7.8 mm Bio-Sil SEC Guard; Bio-Rad, Hercules, CA, USA). Neither degradation nor aggregation was observed for pure pepsin, pure chymosin or the mixture, even after storage for several weeks at 4°C. In subsequent experiments, protein solutions were discarded after one month of storage at 4°C.

3.3. Immobilization of pepstatin A

The IAV membrane surface contains an imidazole moiety which is displaced by amino nucleophiles during immobilization to form a stable amide bond [16,23]. Using the diffusional immobilization method recommended by the manufacturer [24], 1,6-hexanediamine was coupled to the membrane. Pepstatin A was attached to the free amine group of 1,6-hexanediamine using the carbodiimide method of Fu [18], except that for membrane compatibility *n*-butanol was used as the solvent for pepstatin A. After being washed sequentially with *n*-butanol, ethanol, water and loading buffer, IAV membrane discs with immobilized pepstatin A were ready for use.

3.4. Batch adsorption experiments

Sorption kinetics and adsorption isotherms of pepsin and chymosin were measured in a batch system. All the experiments were conducted in clean 150-ml glass beakers at room temperature.

Adsorption isotherm

Fifteen IAV membranes with immobilized pepstatin A were incubated with 15 ml of protein solution having different concentrations. The incubation time was over 4 h for chymosin, and over 6 h for pepsin. Final protein concentrations were determined from the measured absorbance at 280 nm using a spectrophotometer (Cary 1 UV–Vis; Varian Instrument Group, Sugarland, TX, USA) and the extinction coefficients are listed in Table 1.

Association rate constant determination

The association rate constant was determined at room temperature using 30 ml of protein solution at concentrations of 0.28 and 0.16 mg/ml for pepsin, and at 0.53 and 0.36 mg/ml for chymosin. The protein solution and 15 dry IAV membranes were added to a 150-ml beaker, then the beaker was covered with Parafilm and shaken by hand. Aliquots of 1 ml were removed at selected time intervals and analyzed for protein concentration, and then returned to the beaker.

Dissociation rate constant determination

Proteins were labeled with the fluorescent reagent DTAF using labeling procedures from Fu [18]. The labeled protein was separated from the unreacted fluorescent reagent using a gel-filtration column (XK 26/40; Pharmacia, Piscataway, NJ, USA) packed with Sephacryl beads (S-200-HR, Sigma). The column was connected to an absorbance detector set at 280 nm (UA-5, ISCO), a fluorescence detector with a 490-nm filter for excitation and a 510–650-nm filter for emission (FL-2, ISCO), and a pump consisting of a speed-controlled motor (Model 7520-25; Cole-Parmer, Chicago, IL, USA) driving a positive-displacement pump head (Model RH0CKC; Fluid Metering, Oyster Bay, NY, USA). The purified labeled protein solutions were filtered with 0.45-μm filters prior to use.

The 15 dry IAV membranes were incubated with 15 ml of fluorescently labeled protein solution in a beaker overnight. The equilibrium concentration of the incubated labeled protein solution was determined using the spectrophotometer, and the membranes were then washed with washing buffer to remove unbound protein. Washing was conducted using the flow system which will be described in the next section. When the effluent absorbance from the flow system

reached a stable value, washing was stopped. An aliquot of 20 ml of unlabeled protein solution at a concentration 10 times the equilibrium concentration was added to a clean 150-ml beaker by pipette. The washed and wet membranes were then immersed into the beaker containing unlabeled protein solution. The contents of the beaker were mixed by manual shaking. A 2-ml sample was taken for fluorescence analysis at each time increment and then returned to the beaker. The protein solution was analyzed using a fluorometer (Deltascan Model 4000; Photon Technology International, South Brunswick, NJ, USA) and excitation and emission wavelengths of 492 and 513 nm, respectively.

3.5. Flow experiments

The equipment for the flow experiments included the positive-displacement pump described above, the Amicon membrane holder, an absorbance detector with a built-in chart recorder (UA-5, ISCO) and a datalogger (Model 50; Electronic Controls Design, Milwaukie, OR, USA). A fraction collector (Retriever II, ISCO) was used to collect effluent samples for the binary-solute separations. All experiments were conducted at room temperature.

The membrane holder was assembled from the bottom up in the order [25]: bottom part of the holder, screen, 4 regenerated cellulose (RC) membranes, 15 IAV membranes, 4 RC membranes, O-ring and finally the top part of the holder. The RC membranes (SM11607; Sartorius, Bohemia, NY, USA) served as flow distributors, and had a pore size of 0.2 μm and a thickness of 80 μm. The top part of the holder was screwed very tightly into the bottom part to compress the O-ring, which prevented fluid from leaking laterally towards the wall of the housing. Prior to experiments, air bubbles trapped in the holder were eliminated using the built-in vent in the top part of the holder while pumping buffer through the holder.

To determine the flow-rate, the effluent solution was collected through the loading stage in the single-solute experiment. The mass of the collected solution was measured and was converted to volume. The density of protein solution was 1.03 g/ml. The calculated loading volume divided by the loading time (collecting time) was equal to the flow-rate. The same procedure was repeated several times to assure the accuracy of the measured flow-rate. In the binary-solute experiments, the same pump settings as in the single-solute experiments were used to achieve the desired flow-rate.

Non-adsorption breakthrough curve measurement

The effect of dead volume mixing in the flow system was determined by measuring the breakthrough curve for a feed solution in which the protein did not adsorb to the membranes. The 15 IAV membranes were inserted as a stack into the membrane holder, sandwiched between the 8 RC membranes. The non-adsorbing solution for this experiment was 0.4 mg/ml pepsin in 0.1 *M* sodium phosphate pH 9.7 buffer. Pepsin was denatured at this pH and did not bind to the immobilized ligand. The volume loaded was 42 ml at a flow-rate of 1 ml/min. The washing buffer was 0.1 *M* sodium phosphate pH 9.7.

Breakthrough curve measurement

The membrane discs (4 RC/15 IAV/4 RC) were placed in the holder and equilibrated with loading buffer. In the single-solute experiments, 97 ml of protein solution were pumped through the membrane holder at flow-rate of 1 ml/min. The feed solutions were 0.4 mg/ml pepsin or 0.4 mg/ml chymosin. The protein absorbance was detected at 280 nm, and recorded by the datalogger. After loading, about 20 ml of washing buffer were pumped through the discs until the absorbance returned to baseline. Elution buffer (0.01 *M* sodium phosphate, pH 12) was used to elute the bound protein from the membranes. A higher flow-rate (4 ml/min) was used for elution because the elution buffer had a higher pH than the recommended pH range (4–10) for IAV membranes [24]. Elution was stopped when the absorbance returned to baseline. Because it was difficult to elute chymosin from membranes using only elution buffer, membranes containing bound chymosin were rinsed with more than 40

ml of 10 mg/ml pepsin in 0.5 *M* glycine buffer pH 3 until the breakthrough curve reached a stable value. At this pH, pepsin binds to pepstatin A very strongly and displaces all the bound chymosin from the membranes. Then, elution buffer was used to completely remove pepsin from the membranes. Lastly, loading buffer was used to rinse the membranes after elution. The membranes were stored in the holder for a short time period when experiments were conducted, and were stored in a clean 150-ml beaker with the loading buffer for longer time periods.

In the binary-solute experiments, two feed solution concentrations were used: either 0.1 mg/ml pepsin and 0.4 mg/ml chymosin, or 0.4 mg/ml pepsin and 0.1 mg/ml chymosin. Flow-rates of 1 ml/min were used with the same experimental setup as that in the single-solute experiments. In the loading stage, 97 ml of the protein mixture were pumped through the membrane cartridge. In the washing stage, 20 ml washing buffer were loaded. The fraction collector was employed to collect 2-ml fractions of effluent solution. The effluent fractions and the feed solution were analyzed by HPLC. The HPLC system, described above, was calibrated at 280 nm using samples of pure protein solutions at selected concentrations. The volume of the HPLC injection loop was 50 μl. The mobile phase was 0.002 *M* Na_2HPO_4, 0.005 *M* Na_2SO_4, 0.1 *M* KCl with 0.005% NaN_3, pH 6.2 [26]. The mobile-phase flow-rate was 1 ml/min. The elution procedure for the mixture of pepsin and chymosin is the same as that for chymosin. First, membranes in the flow system were loaded with 10 mg/ml pepsin in 0.5 *M* glycine buffer pH 3 until the breakthrough curve reached a stable value. Then, 0.01 *M* sodium phosphate pH 12 elution buffer was used to completely remove pepsin from membranes. Lastly, loading buffer was used to rinse and store the membranes.

4. Results

4.1. Batch performance

Single-solute adsorption isotherm

The experimental adsorption isotherms for pure pepsin and chymosin are plotted in Fig. 1. The bound protein concentration based on solid membrane volume (c_s) was plotted against the free protein concentration in solution (c) at equilibrium. To determine the dissociation equilibrium constant (K_d) and maximum binding capacity (c_1), these data were fitted to the single-solute Langmuir isotherm equation

$$c_s = \frac{cc_1}{K_d + c} \tag{9}$$

The fitted values were: $K_d = 9(2) \cdot 10^{-6}$ *M* and $c_1 = 2.3(0.1) \cdot 10^{-4}$ *M* for pepsin; $K_d = 4(1) \cdot 10^{-6}$ *M* and $c_1 = 2.9(0.2) \cdot 10^{-4}$ *M* for chymosin, where values in parentheses indicate the standard error.

Single-solute association

The association rate data are presented in Fig. 2. To determine the association rate constant

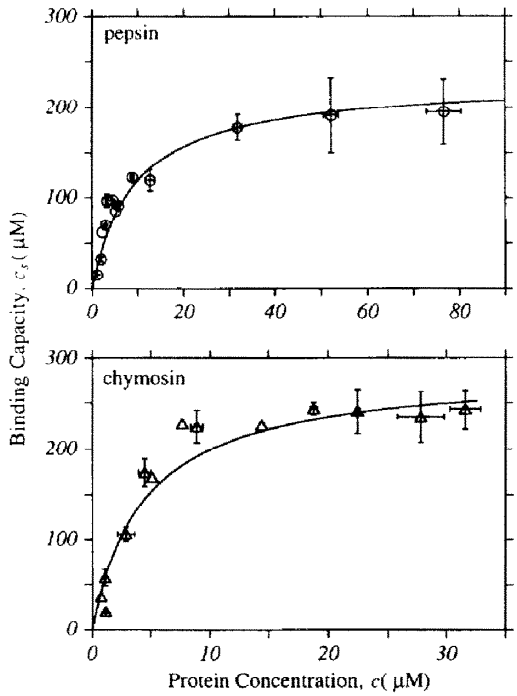

Fig. 1. Single-solute adsorption isotherms for pepsin (○) and chymosin (△) using 15 IAV membranes. The loading buffer was 0.01 *M* imidazole with 1 *M* NaCl at pH 6. The data were fitted by least-squares to Eq. 9 and plotted as solid lines. Error bars span 2 S.D., and points without error bars were measured in only one trial.

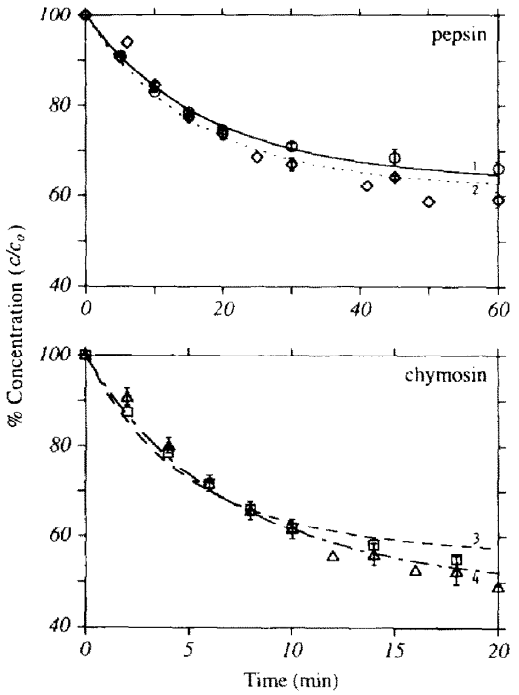

Fig. 2. Single-solute association curves using 15 IAV membranes. For pepsin, the feed solution concentrations were 0.28 mg/ml (○) and 0.16 mg/ml (◇). For chymosin, the feed solution concentrations were 0.53 mg/ml (□) and 0.36 mg/ml (△). The data were fitted by least-squares to Eq. 10: $c_0 = 0.28$ mg/ml pepsin (curve 1), $c_0 = 0.16$ mg/ml pepsin (curve 2), $c_0 = 0.53$ mg/ml chymosin (curve 3) and $c_0 = 0.36$ mg/ml chymosin (curve 4).

(k_a), the data were fitted to the Langmuir kinetic equation [27]

$$\frac{c}{c_0} = 1 - \frac{2c_1 \sinh\left(\frac{\hat{V}G}{2} \cdot k_a t\right)}{G \cosh\left(\frac{\hat{V}G}{2} \cdot k_a t\right) + B \sinh\left(\frac{\hat{V}G}{2} \cdot k_a t\right)} \quad (10)$$

where

$$B = \frac{c_0}{\hat{V}} + c_1 + \frac{K_d}{\hat{V}} \quad (11)$$

$$G = \left(B^2 - \frac{4c_0c_1}{\hat{V}}\right)^{1/2} \quad (12)$$

$$\hat{V} = \frac{(1-\epsilon)(\text{total membrane volume})}{(\text{experimental solution volume})} \quad (13)$$

The fitted values were: for pepsin, $k_a = 43(4)$ M^{-1} s^{-1} when $c_0 = 0.28$ mg/ml, and $k_a = 49(8)$ M^{-1} s^{-1} when $c_0 = 0.16$ mg/ml; and for chymosin, $k_a = 150(30)$ M^{-1} s^{-1} when $c_0 = 0.53$ mg/ml, and $k_a = 127(8)$ M^{-1} s^{-1} when $c_0 = 0.36$ mg/ml. Four equilibrium points were obtained from these association experiments, and plotted in the corresponding adsorption isotherms of Fig. 1.

The time scales for protein diffusion to and association with the ligand were calculated and compared. The time scale for protein diffusion was l^2/D [28]. The diffusion path length (l) was 70 μm, one half the thickness of an individual membrane. Thus, the time scale for protein diffusion was 0.9 min for both pepsin and chymosin. The average time scale for protein association with the ligand ($1/k_a c_0$) was 70 min for pepsin, and 10 min for chymosin. The time scale for protein diffusion was negligible in comparison to the time scale for protein association with the ligand.

Single-solute dissociation

The dissociation rate data were fitted to a first-order kinetic equation [1,27]

$$F = F_{max}(1 - e^{-k_d t}) \quad (14)$$

where F was the measured fluorescence in the solution over time, and F_{max} was the maximum fluorescence attained at long time. To normalize each experimental data set in terms of F/F_{max} (%), the data were fitted to Eq. 14 to determine F_{max}. Then F/F_{max} was plotted in Fig. 3, and the data were fitted to Eq. 14 to determine k_d. The fitted values were: $k_d = 4.5(0.7) \cdot 10^{-4}$ s^{-1} for pepsin and $k_d = 6.1(0.8) \cdot 10^{-4}$ s^{-1} for chymosin. These values of k_d along with the experimentally determined dissociation equilibrium constant were used to calculate values for k_a ($= k_d/K_d$) of 50 M^{-1} s^{-1} for pepsin and 150 M^{-1} s^{-1} for chymosin. The calculated values of k_a were within one standard error of the values determined from the data of Fig. 2.

The time scale for protein diffusion (0.9 min)

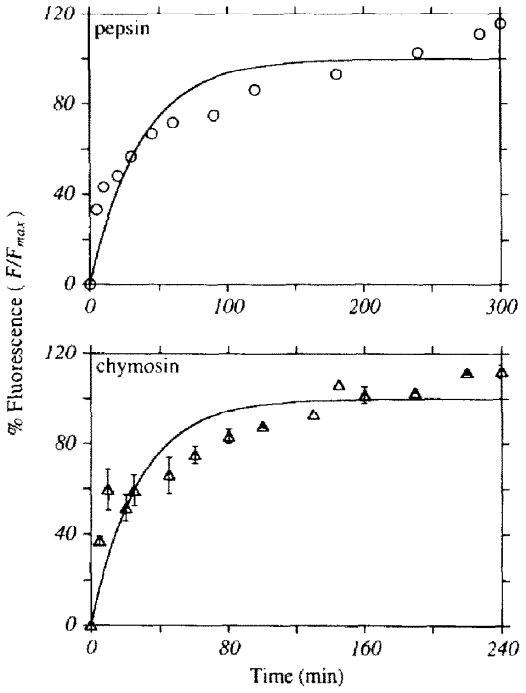

Fig. 3. Single-solute dissociation curves using 15 IAV membranes. The membranes were equilibrated with the fluorescently labeled protein solution first, and then excess unlabeled protein was used to displace the bound labeled protein. Eq. 14 was used to determine the F_{max} and k_d values, and the fitted curves are presented as solid lines for pepsin (○) and chymosin (△).

was negligible compared to the average time scale for protein dissociation ($1/k_d$) of 30 min.

4.2. Breakthrough curves

Non-adsorption experiments

The breakthrough curve for a non-adsorbing feed solution at a flow-rate of 1 ml/min is presented in Fig. 4. There were delay volume and dead volume mixing effects evident in the breakthrough curves. To simplify the model for this behavior, a model of one plug-flow reactor (PFR) plus one continuous stirred-tank reactor (CSTR) was used as described in the work of Raths [29] on dead volume mixing in an ion-exchange membrane cartridge. The CSTR model was

$$V \cdot \frac{dc_{out}}{dt} = Q(c_{in} - c_{out}) \quad (15)$$

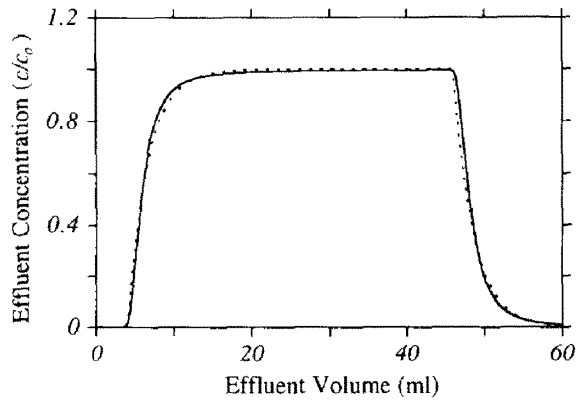

Fig. 4. Non-adsorption breakthrough curves at 1 ml/min for 4 RC/15 IAV/4 RC membranes. Solid line = experimental data; dotted line = model prediction. The model included a plug-flow volume of 2.55 ml for the affinity membranes, a CSTR mixing volume of 2.6 ml, and a plug-flow volume of 1.45 ml for the remainder of the system.

where V is the CSTR volume, Q is the flow-rate through the CSTR, c_{in} is the inlet concentration, and c_{out} is the outlet concentration. The plug-flow model accounted for a delay time (t_{delay}) such that at $t < t_{delay}$ the effluent concentration from the system was zero, and at $t \geq t_{delay}$ the effluent concentration was equal to c_{out} at the time $t - t_{delay}$.

The first temporal moment method was used to determine V and t_{delay} [30]. The mean time the fluid spent in the experimental system was

$$t_{1st\ moment} = \frac{M_1 - \mu_1}{M_0} \quad (16)$$

where M is the moment of effluent concentration and μ is the moment of inlet concentration.

The mean residence volume ($Qt_{1st\ moment}$) consists of all the postulated dead volumes in the membrane system. From Fig. 4, the calculated mean residence volume was 6.6 ml, and the delay volume was 4 ml. Therefore, by difference the CSTR volume was 2.6 ml. The void volume of 15 IAV membranes was 2.55 ml, leaving 1.45 ml as the remaining PFR volume of the system. Accordingly, the dead volume mixing model consisted of 2.55 ml PFR volume for the affinity membranes, 1.45 ml PFR volume for the remainder of the flow system, and 2.6 ml CSTR

volume. The result of the dead volume mixing model was plotted in Fig. 4. The model predictions were nearly identical to the experimental results.

Parameter values used in the affinity-membrane model

The values for the membrane parameters were taken from the manufacturer [16,24]. The porosity, ϵ, was 0.7, and the individual IAV membrane thickness, L, was 140 μm. In this work, 15 membranes were stacked together, resulting in a total thickness of 0.21 cm. The flow-rate used in this work was 1 ml/min. Consequently, using the membrane diameter of 47 mm, the interstitial flow velocity passing through the membrane pores, v, was $1.37 \cdot 10^{-3}$ cm/s. The single-solute isotherm parameters were: $K_d = 9 \cdot 10^{-6}$ M and $c_1 = 2 \cdot 10^{-4}$ M for pepsin; $K_d = 4 \cdot 10^{-6}$ M and $c_1 = 3 \cdot 10^{-4}$ M for chymosin, as determined experimentally (Fig. 1). The association rate constants were: $k_a = 50$ M^{-1} s^{-1} for pepsin and $k_a = 150$ M^{-1} s^{-1} for chymosin, based on experimental results (Fig. 2). The dimensionless number of transfer units (n) was calculated from these values: $n = 0.66$ for pepsin and $n = 2.95$ for chymosin. The dissociation rate constant was calculated from $k_d = k_a K_d$.

The dimensionless separation factor (r) was: 1.3 for 0.1 mg/ml pepsin, 2.3 for 0.4 mg/ml pepsin, 1.7 for 0.1 mg/ml chymosin and 4.0 for 0.4 mg/ml chymosin. The four initial concentrations used experimentally yield dimensionless saturation capacities (m) of 30 (0.1 mg/ml pepsin), 7 (0.4 mg/ml pepsin), 43 (0.1 mg/ml chymosin) and 11 (0.4 mg/ml chymosin), respectively, using the values of ϵ and c_1 described above.

The axial Peclet numbers (Pe) were calculated from the diffusion coefficients (Table 1) and the above values of the parameters v and L, and were: 330 for pepsin and 340 for chymosin.

The model calculations were performed in sequence. First, the affinity-membrane model, Eqs. 1–8, was solved using the PDASAC software package. This yielded the breakthrough curves which included only the effects of slow and competitive sorption kinetics, and axial diffusion. The effluent concentrations were then used as the inlet concentrations for the CSTR mixing model, Eq. 15, which was solved using a finite-difference method. This included the effects of dead volume mixing into the breakthrough curves from the affinity-membrane model. Lastly, the PFR model was used to shift the results to longer times. This accounted for the delay time which resulted from plug flow through the dead volume in the flow system. The final result of the calculations was breakthrough curves which included the effects of slow and competitive sorption kinetics, axial diffusion, and CSTR mixing and plug flow in the dead volume of the flow system.

Single-solute breakthrough curves including adsorption

Experimental single-solute breakthrough curves at a flow-rate of 1 ml/min are shown in Fig. 5. For pepsin, protein first appeared in the effluent at an effluent volume of 2.5 ml. The effluent concentration rose quickly to 80% of the feed solution concentration after 20 ml effluent volume, and then increased slowly towards the feed solution concentration. The breakthrough curve for chymosin had a front shoulder after emerging at an effluent volume of 4.5 ml. The effluent concentration increased to 30% of the feed solution concentration at 20 ml effluent volume, and then increased to 80% at 30 ml effluent volume.

In Fig. 5, the curves predicted from the model were in close agreement with the experimental curves early on, but the model curves fell somewhat below the experimental curves in the range of 20 to 40 ml effluent volume. After 80 ml effluent volume, both the model and experimental curves approached the feed solution concentration. However, the model curves reached the level of the feed solution concentration, and the experimental curves fell slightly short of this level. Generally, the differences between the predictions and the experimental data were small. The predictions of the model were sensitive to doubling and halving the values of the parameters used for the sorption isotherm and

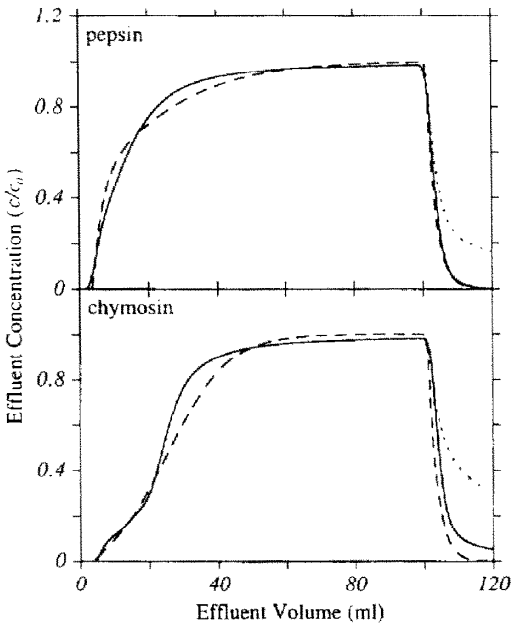

Fig. 5. Single-solute breakthrough curves for pepsin and chymosin at 1 ml/min. The measured curves (solid lines) were plotted along with predictions from the model (broken lines). Two washing models were used: without sorption during washing (broken lines) and with sorption during washing (dotted lines).

kinetics (results not shown). Values different than the experimentally determined values produced inaccurate model predictions.

In Fig. 5, the washing curves predicted using the model with sorption (Eq. 3) contained a long tail due to protein dissociation. The curves predicted using the model without sorption (Eq. 4) predicted fast washing, which more closely resembled the experimental curves. The washing process in affinity-membrane separations was best described by neglecting protein sorption kinetics.

Binary-solute breakthrough curves including adsorption

Experimental binary-solute breakthrough curves are presented in Figs. 6d and 7d. In both experiments, pepsin appeared first in the effluent. After an additional 5 ml of effluent volume, chymosin appeared in the effluent. Chymosin had a sharper breakthrough curve when its concentration was elevated compared to pepsin as shown in Fig. 6d.

The breakthrough curves were compared with the predictions of the model. The equilibrium and kinetic parameters used in the model were the same as those used for the single-solute breakthrough curves (Fig. 5). For both feed solution compositions, the predicted curves fitted the experimental data well.

Affinity-membrane model and local-equilibrium theory

In Figs. 6 and 7, model predictions using (a) local-equilibrium theory, (b) local-equilibrium theory with CSTR mixing, (c) affinity-membrane model and (d) affinity-membrane model with CSTR mixing were plotted along with the experimental data. Local-equilibrium theory was compared to the experimental data in order to distinctly isolate the effects of dead volume mixing, slow sorption kinetics, and interactive competition due to differences in either affinity strength or sorption kinetics. Local-equilibrium theory is based on thermodynamics, and does not include any mass-transfer effects. Local-equilibrium separations occur when the sorption kinetics are fast enough to allow equilibrium to exist between protein and ligand at all binding sites [9].

The predictions from local-equilibrium theory contained two square-wave plateaus as shown in Figs. 6a and 7a. The first plateau contained only pepsin, the lower-binding-strength protein. In the beginning of loading, both pepsin and chymosin completely bound to the ligand and no protein emerged in the effluent. As the binding sites were saturated with protein, the stronger-binding chymosin started to displace bound pepsin off the membrane surface. This displacement resulted in an effluent concentration of pepsin higher than the feed solution concentration of pepsin. Displacement was more rapid and noticeable for ideal local-equilibrium behavior when the concentration of strong-binding chymosin was elevated. When the membrane reached equilibrium, chymosin emerged in the effluent and pepsin displacement stopped. After this point the effluent concentration of both

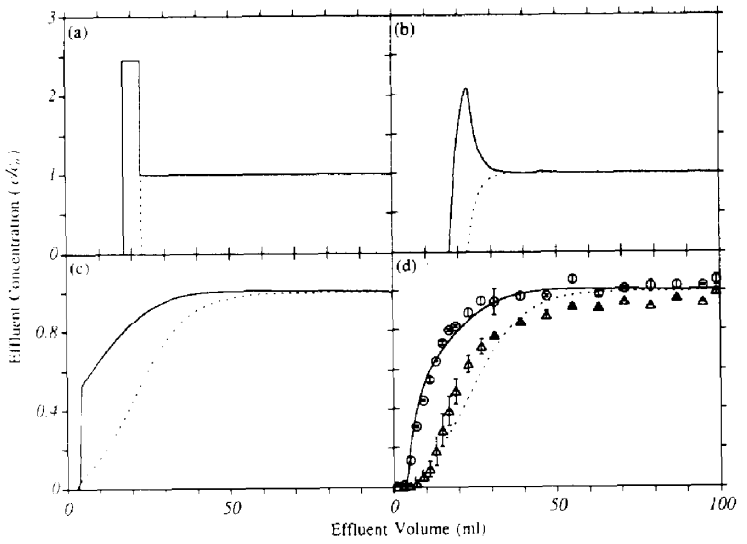

Fig. 6. Comparison of experimental breakthrough curves for a feed solution containing 0.1 mg/ml pepsin (○) and 0.4 mg/ml chymosin (△) at 1 ml/min to predictions (solid lines = pepsin; dotted lines = chymosin) made using (a) local-equilibrium theory, (b) local-equilibrium theory with CSTR mixing, (c) affinity-membrane model and (d) affinity-membrane model with CSTR mixing.

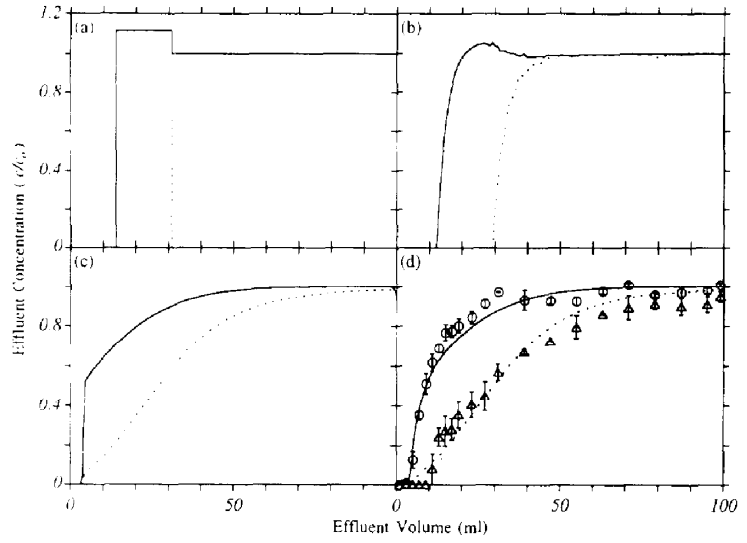

Fig. 7. Comparison of experimental breakthrough curves for a feed solution containing 0.4 mg/ml pepsin (○) and 0.1 mg/ml chymosin (△) at 1 ml/min to predictions (solid lines = pepsin; dotted lines = chymosin) made using (a) local-equilibrium theory, (b) local-equilibrium theory with CSTR mixing, (c) affinity-membrane model and (d) affinity-membrane model with CSTR mixing.

proteins was equal to the feed solution concentration.

As shown in Figs. 6b and 7b, when CSTR mixing in the flow system was added to the predictions from local-equilibrium theory, the mixing effect broadened the edges of square waves and decreased the effluent concentration during displacement. The mixing effect degraded the separation performance.

The experimental results using affinity membranes (Figs. 6d and 7d) bore no resemblence to either local-equilibrium theory (Figs. 6a and 7a) or this theory with CSTR mixing (Figs. 6b and 7b). Although including CSTR mixing in the affinity-membrane model gave the best predictions (Figs. 6d and 7d), predictions made without the CSTR mixing model were close to the experimental data (Figs. 6c and 7c). The dominant effect was the slowness of the interactive and competitive sorption kinetics.

The sharp or sudden increase in the calculated effluent concentration for pepsin in Figs. 6c and 7c was the result of slow sorption kinetics. The residence time of the fluid in the membrane was 2.55 min, which was too short for pepsin to bind to the membrane. Therefore, pepsin emerged in the effluent immediately after the delay volume of the system of 4 ml. However, chymosin, which had an association rate constant three-times greater than that of pepsin, did bind to the membrane in this residence time. Therefore, there was not a sharp increase in the calculated effluent concentration for chymosin.

5. Discussion

In this work, an affinity-membrane model of breakthrough curves was validated by extensive experimentation. Sorption equilibrium isotherm and kinetic parameters were measured in batch experiments. These measurements were completely independent of the affinity-membrane model. Breakthrough curves were then measured and compared to the predictions made using the model. For both single-solute and binary-solute separations, the predictions using the model were in good agreement with the experimental breakthrough curves.

Predictions made using either local-equilibrium theory or the affinity-membrane model were compared to the experimental data. The predictions made using the binary-solute affinity-membrane model closely matched the experimental data, and predictions made using local-equilibrium theory were a distinct mismatch. This confirmed that slow sorption kinetics were the dominant cause of broad breakthrough curves in affinity-membrane separations.

In addition to slow sorption kinetics, it is possible that broad breakthrough curves may result from two mass-transfer effects analyzed in our previous work [8]: boundary-layer mass transfer (BLMT) and axial diffusion. Due to the small pore size of the membrane matrix used in this research, BLMT was fast and did not affect the shape of the breakthrough curves [10,31]. Axial diffusion dominates membrane performance at low flow velocity. When Pe is smaller than 40, axial diffusion causes broad breakthrough curves [8]. Because Pe was 330 for pepsin and 340 for chymosin, axial diffusion did not affect the shape of the breakthrough curves.

Lower flow-rates would be necessary to to achieve sharper breakthrough curves. Operating conditions which produce sharp breakthrough curves from affinity membranes have been defined previously using the affinity-membrane model [8]. Based on the parameter values determined experimentally in this work, flow-rates of 0.013 ml/min for pepsin and 0.053 ml/min for chymosin would be required to achieve sharp breakthrough curves in the experiments of Fig. 5. At the 1 ml/min flow-rate used in these experiments, slow sorption kinetics would be expected to dominate affinity-membrane performance and produce broad breakthrough curves.

This work employed the Langmuir model to determine the sorption equilibrium and rate constants. Although the Langmuir model did not perfectly fit the batch experimental data, the affinity-membrane model using these fitted parameter values was a good predictor of experimental breakthrough curves from the mem-

brane. Perhaps because the flow system operated far from equilibrium, the Langmuir model needs only to accurately describe the association kinetics at short times in order to produce accurate predictions of the breakthrough behavior. The residence time of the fluid in the affinity membranes was 2.55 min. From Fig. 2, at this residence time, the system was not only far from equilibrium for both pepsin and chymosin, but also the Langmuir model was able to accurately describe the association kinetics at this short time. This made the use of Langmuir model valid for this affinity system.

For other adsorptive membrane systems which may operate closer to equilibrium there is a need for more accurate multi-solute sorption models in order to ensure the predictions of the affinity-membrane model are equally valid. Ion-exchange membranes are an example of such a system. In the work of Weinbrenner and Etzel [32], α-lactalbumin and bovine serum albumin were separated using an ion-exchange membrane. The separation performance qualitatively matched the predictions from local-equilibrium theory together with the CSTR mixing model. Apparently, the ionic interaction between protein and ligand was fast enough to allow local-equilibrium behavior to occur, but small amounts of mixing in the flow system impaired attainment of exact local-equilibrium behavior in the breakthrough curve. Further theoretical and experimental research on the thermodynamics and kinetics of multi-solute sorption are crucial to developing a better understanding of adsorptive-membrane separations such as this one.

In practice, affinity membranes are frequently used to separate a desired biomolecule from a crude solution which may contain extracellular and intracellular components, salts, detergents and other undesired materials. These components may not bind with high affinity to the membrane, but may be present in much higher concentration than the desired component, and may have greater association rate constants for the ligand. Consequently, contaminating low-affinity components may compete with the desired high-affinity component for binding sites.

This work demonstrated that under carefully chosen and controlled conditions, the performance of affinity-membrane systems can be predicted well using the affinity-membrane model. Thus, the fundamental factors governing affinity-membrane performance were identified as slow and competitive sorption kinetics, axial diffusion and dead volume mixing. However, realistic modelling of affinity-membrane separations using crude solutions will have to await experimentally validated mathematical models of the fundamental sorption behavior occurring in these complicated solutions.

Symbols

B	parameter defined in Eq. 11
c	solute concentration in the mobile phase, M
c_l	ligand capacity in the stationary phase based on the solid volume, M
c_0	feed solute concentration in the mobile phase, M
c_s	concentration of solute–ligand complex in the stationary phase, M
C	dimensionless solute concentration in the mobile phase ($= c/c_0$)
C_s	dimensionless concentration of solute–ligand complex in the stationary phase ($= c_s/c_l$)
D	axial diffusion coefficient, cm^2/s
E	extinction coefficient
F	fluorescence in the solution
G	parameter defined in Eq. 12
k_a	association rate constant, $M^{-1}\ s^{-1}$
k_d	dissociation rate constant, s^{-1}
K_d	dissociation equilibrium constant, M ($= k_d/k_a$)
l	diffusion path, cm
L	membrane thickness, cm
m	dimensionless saturation capacity [$= (1-\epsilon)c_l/\epsilon c_0$]
M_n	nth moment of the effluent concentration
M_r	molecular mass
n	dimensionless number of transfer units [$= (1-\epsilon)c_l k_a L/\epsilon v$]

Pe	axial Peclet number ($=vL/D$)
pI	isoelectric point
Q	flow-rate, ml/s
r	dimensionless separation factor ($=1+c_0/K_d$)
t	time, s
v	interstitial flow velocity, cm/s
V	CSTR volume, ml
$\hat{V}$	parameter defined in Eq. 13
z	axial distance along the membrane, cm

Greek letters

ϵ	porosity of membrane
ζ	dimensionless spatial variable ($=z/L$)
μ_n	nth moment of the inlet concentration
τ	dimensionless time ($=vt/L$)

Subscripts

1st moment	first temporal moment
delay	plug-flow delay
i, j	solute index
in	inlet
max	maximum value
out	outlet
w	washing

Acknowledgements

Funding for this work was provided by Grant BCS-9109577 from the National Science Foundation and Hatch Grant 3318 from the United States Department of Agriculture. Paul Soltys supplied important technical advice while reviewing the manuscript.

References

[1] F.H. Arnold, H.W. Blanch and C.R. Wilke, *Chem. Eng. J.*, 30 (1985) B9.
[2] S. Brandt, R.A. Goffe, S.B. Kessler, J.L. O'Connor and S.E. Zale, *Bio/Technology*, 6 (1988) 779.
[3] K.-G. Briefs and M.-R. Kula, *Chem. Eng. Sci.*, 47 (1992) 141.
[4] M. Unarska, P.A. Davies, M.P. Esnouf and B.J. Bellhouse, *J. Chromatogr.*, 519 (1990) 53.
[5] Dj. Josić, J. Reusch, K. Löster, O. Baum and W. Reutter, *J. Chromatogr.*, 590 (1992) 59.
[6] J.A. Gerstner, R. Hamilton and S.M. Cramer, *J. Chromatogr.*, 596 (1992) 173.
[7] T.B. Tennikova and F. Svec, *J. Chromatogr.*, 646 (1993) 279.
[8] S.-Y. Suen and M.R. Etzel, *Chem. Eng. Sci.*, 47 (1992) 1355.
[9] S.-Y. Suen, M. Caracotsios and M.R. Etzel, *Chem. Eng. Sci.*, 48 (1993) 1801.
[10] M. Nachman, A.R.M. Azad and P. Bailon, *J. Chromatogr.*, 597 (1992) 155.
[11] H.-C. Liu and J.R. Fried, *AIChE J.*, 40 (1994) 40.
[12] M. Kim, K. Saito, S. Furusaki, T. Sato, T. Sugo and I. Ishigaki, *J. Chromatogr.*, 585 (1991) 45.
[13] G.C. Serafica, J. Pimbley and G. Belfort, *Biotech. Bioeng.*, 43 (1994) 21.
[14] P.V. Danckwerts, *Chem. Eng. Sci.*, 2 (1953) 1.
[15] M. Caracotsios and W.E. Stewart, *Comput. Chem. Eng.*, (1994) in press.
[16] L.A. Blankstein and L. Dohrman, *Am. Clin. Prod. Rev.*, 11 (1985) 33.
[17] T.-J. Fu and A. Carlson, presented at the *24th ACS Mid-Atlantic Regional Meeting, Madison, NJ, 1990*, paper 165.
[18] T.-J. Fu, *M.S. Thesis*, Pennsylvania State University, University Park, PA, 1988.
[19] T.-J. Fu, *Ph.D. Thesis*, Pennsylvania State University, University Park, PA, 1992.
[20] C.A. Ernstrom and N.P. Wong, in B.H. Webb, A.H. Johnson and J.A. Alford (Editors), *Fundamentals of Dairy Chemistry*, AVI Publishing, Westport, 2nd ed., 1974, Ch. 12.
[21] H. Edelhoch, *J. Am. Chem. Soc.*, 79 (1957) 6100.
[22] R. Djurtoft, B. Foltmann and A. Johansen, *Compt. Rend. Trav. Lab. Carlsberg*, 34 (1964) 287.
[23] A.J. Weiss, S.A. McElhinney and L.A. Blankstein, *BioTechniques*, 7 (1989) 1012.
[24] Millipore, *Immobilon™ Tech Protocol*, Bedford, MA, 1987.
[25] S.-Y. Suen, *Ph.D. Thesis*, University of Wisconsin, Madison, WI, 1994.
[26] A. Carlson and R. Nagarajan, *Biotechnol. Prog.*, 8 (1992) 85.
[27] W.C. Olson, T.M. Spitznagel and M.L. Yarmush, *Mol. Immunol.*, 26 (1989) 129.
[28] R.B. Bird, W.E. Stewart and E.N. Lightfoot, *Transport Phenomena*, Wiley, New York, 1960.
[29] K.-R. Raths, *M.S. Thesis*, University of Wisconsin, Madison, WI, 1992.
[30] E.N. Lightfoot, A.M. Lenhoff and R.L. Rodriguez, *Chem. Eng. Sci.*, 37 (1982) 954.
[31] D.D. Frey, R. van de Water and B. Zhang, *J. Chromatogr.*, 603 (1992) 43.
[32] W.F. Weinbrenner and M.R. Etzel, *J. Chromatogr. A*, 662 (1994) 414.